Beta-Decay Half-Lives and Neutron-Emission Probabilities of Very Neutron-Rich Y to Tc Isotopes

T. Mehren, B. Pfeiffer, S. Schoedder, and K.-L. Kratz*
Institut für Kernchemie, Universität Mainz, D-55099 Mainz, Germany

M. Huhta,† P. Dendooven, A. Honkanen, G. Lhersonneau, M. Oinonen, J.-M. Parmonen, H. Penttilä, A. Popov,‡ V. Rubchenya,§ and J. Äystö
Department of Physics, Accelerator Laboratory, University of Jyväskylä, FIN-40351 Jyväskylä, Finland
(Received 26 February 1996)

Neutron-rich $_{39}$Y to $_{43}$Tc isotopes have been produced by fission of uranium with a 50 MeV H_2^+ beam. Beta-decay half-lives, delayed neutron-emission probabilities, and production yields have been measured and compared with theory. Beta decay of 4 new isotopes is reported, and the β-delayed neutron-emission mode has been discovered for 12 isotopes of the elements niobium and technetium. The results compared to quasiparticle random phase approximation predictions indicate the increasing importance of fast β transitions to high-lying states of nuclei with large neutron excess. [S0031-9007(96)00640-0]

PACS numbers: 23.40.Hc, 21.10.Tg, 25.85.Ge, 27.60.+j

The study of nuclei with extreme neutron to proton ratios is of growing interest due to indications of new nuclear-structure phenomena near the drip lines [1] unpredicted by models mainly adopted for nuclei in the valley of stability, as well as due to strong connections with astrophysics [2,3]. From recent attempts to reproduce the isotopic abundance distribution in the solar system, constraints on the nuclear structure of very neutron-rich nuclei were derived [2]. For example, as a consequence of quenching of the $N = 82$ magic neutron shell [1], nuclei around $A \simeq 120$ were "requested" to be less bound and less deformed than predicted by recent macroscopic-microscopic models [4,5]. This has, indeed, been observed for a number of neutron-rich even-even Ru nuclides [6–8].

A consistent description of the restoration of deformation in the $Z > 38$, $N > 60$ transitional region still demands further insights into the proton-neutron residual interaction which determines the development of nuclear structure. In particular, dramatic changes in the position of single-particle states depending on the occupancy of spin-partner orbitals have been revealed in recent years leading to new subshell closures with correlated changes in nuclear ground states and lower neutron separation energies S_n (see, e.g., discussion in [9]).

Gross β-decay properties, such as the β-decay half-life ($T_{1/2}$) and the delayed neutron-emission probability (P_n), are the easiest measurable quantities for isotopes very far from stability produced with low production yields. Although being integral parameters, they do contain important nuclear-structure information; i.e., $T_{1/2}$ is sensitive to the low-lying β strength, whereas the P_n value carries information on the strength just beyond S_n (see, e.g., [10]). In comparing experimental results with predictions from shell models, such as the quasiparticle random phase approximation (QRPA) for Gamow-Teller (GT) β decay [11], one obtains first indications on possible nuclear-structure features associated with high neutron excess. In addition, the systematics of experimental observables such as $T_{1/2}$, P_n, and S_n values provide an important basis for reliable extrapolations up to the *r*-process path, which is not well understood in the $110 \leq A \leq 120$ region considered here [2].

Production cross sections of neutron-rich nuclei very far from the valley of stability are in general very low, so that experimental techniques have to be stressed to their limits. For medium-heavy nuclei with $A > 70$, fission of heavy actinides is still the preferred production mode. In the past, most of the studies applied low-energy fission with the strongly asymmetric mass distribution. Identification and detailed studies of a large number of new neutron-rich nuclei have been possible with charged-particle-induced fission [12], and more recently using projectile fission of high-energy U beams [13].

In this work, we report on the production and the β-delayed-neutron decay mode of highly neutron-rich isotopes of yttrium, niobium, and technetium lying at and beyond the boundary of previously known nuclei. The isotopes under investigation were produced in fusion-fission reactions [14] by bombarding a U target with a 50 MeV H_2^+ beam of 6–8 μA intensity from the $K = 130$ MeV cyclotron at the University of Jyväskylä. The newly upgraded ion guide separator (IGISOL) was used to produce and separate isobarically pure beams of primary fission products with delay time of the order of milliseconds only [15]. Because of nonselectivity with respect to *Z*, the detection of the most neutron-rich species of each isobar by β- and γ-spectroscopic methods is difficult because of copiously produced isobaric contaminants. The highest sensitivity to identify these exotic isotopes is provided by spectroscopy of β-delayed neutrons. Because of odd-even effects in S_n values, a high sensitivity is obtained especially for odd-*Z* precursors (with "low" S_n's) compared to neigh-

 0031-9007/96/77(3)/458(4)$10.00

boring even-Z elements (with "high" S_n's). The combination of the usually high P_n values of very neutron-rich isotopes and high-efficiency neutron counting provided by the neutron long-counter technique offers excellent means to probe the decay characteristics of exotic nuclei produced in fission.

The 40 keV beam of mass separated short-lived nuclei was implanted into a collection tape positioned inside the 4π neutron long counter. The implantation position was also viewed by a thin plastic scintillator (NE110) for detecting β particles or by a planar Ge detector for detecting γ rays. To reduce the β and γ background of longer-lived isobaric activities, the collection tape was moved in preset time intervals. Each n, β, or γ signal collected was associated with the time of occurrence after the pulsing of the separator beam. The neutron long counter consisted of 42 ^{3}He ionization chamber tubes, which were arranged in two concentric rings in a polyethylene block surrounding the implantation point. The efficiency of the counter was determined with the calibrated Am/Li and ^{252}Cf neutron sources to be $(24.9 \pm 0.2)\%$. It is nearly energy independent due to the thermalization of the neutrons. The neutron background rate was 0.7 count/s. In order to further reduce the background, delayed coincidences between neutrons and β particles were taken, following the technique of Reeder *et al.* [16]. The efficiency of the β detector was determined repeatedly from the β-neutron coincidence rates of ^{94}Rb and ^{95}Rb, which have well-known P_n values [17]. Depending on the exact geometry of the β detector, its efficiency varied between 5.2% and 12.0%.

The half-lives of the β-delayed neutron precursors were determined from both β-gated and neutron singles multiscaling curves by fitting the total growth-in and decay periods of the time spectra. In all cases, a constant neutron background was included in the fit. For $A = 104$, 109, and 110, two components had to be considered in the fit. Data sets with collection-decay cycles adapted to each of the components were accumulated to disentangle the complex time spectra. In all other cases, only one component was required. As an example, singles neutron growth-in and decay curves for ^{103}Y, ^{108,109}Nb, and ^{112}Tc are shown in Fig. 1.

Neutron branching ratios (P_n values) were determined from the absolute intensities of neutrons, β particles, and βn coincidences from the unfolded decay curves. The $T_{1/2}$ and P_n values, as measured in this work, are given in Tables I and II, respectively. For the isotopes ^{103}Y and $^{108-110}$Nb, the β-decay half-lives are reported for the first time. In all other cases, the half-lives are compared with earlier values determined by β-γ counting. On the average, good agreement is observed. Altogether 13 new P_n values have been measured in this work. In addition, several earlier known branching ratios for yttrium isotopes were remeasured with improved statistics and are compared with literature values [17] in Table II. It should be mentioned that in the former experiments the yttrium activities had been obtained as decay products of primarily separated Rb/Sr activities with much higher delayed-neutron yields. Hence, fitting yttrium as a third weak component led to large systematic uncertainies (for discussion, see, e.g., [16–18]). At IGISOL, however, also refractory elements such as yttrium are obtained as primary ion beams. For the heavy yttrium isotopes, the fission yields of their Rb and Sr isobars are negligible. Hence, the unfolding procedure of the neutron spectra has to take into account only one decay component, thus resulting in P_n values for yttrium with higher reliability.

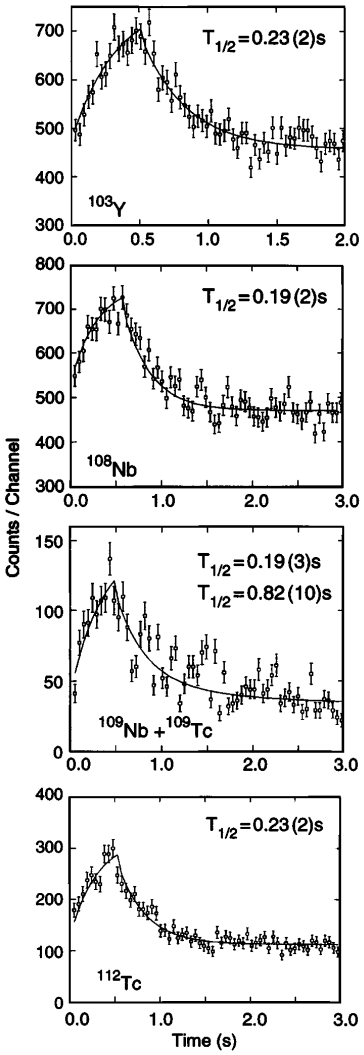

FIG. 1. Singles neutron growth-in and decay curves for ^{103}Y, ^{108}Nb, ^{109}Nb, and ^{112}Tc. The solid curves represent the fit functions taking into account one decay component and a constant background. In the case of $A = 109$, a superposition of two independent components for ^{109}Nb and ^{109}Tc was applied. No neutron activity corresponding to the decay of the intermediate ^{109}Mo could be observed.

The experimental $T_{1/2}$ and P_n values are compared to predictions of the QRPA model in Tables I and II. For these calculations, the masses and ground-state deformations were taken either from the FRDM model [4] or from

TABLE I. List of $T_{1/2}$ results. The QRPA predictions are calculated with masses and deformations from both the FRDM [4] and ETFSI [5] mass models. Experimental masses from [23] replaced the predicted ones whenever known. The literature values are taken from the Nuclear Data Sheets unless otherwise stated.

Isotope	$T_{1/2}^{\mathrm{exp}}$ (s)	$T_{1/2}^{\mathrm{QRPA}}$ FRDM (s)	$T_{1/2}^{\mathrm{QRPA}}$ ETFSI (s)	$T_{1/2}^{\mathrm{Lit.}}$ (s)
$^{94}\mathrm{Kr}_{58}$	0.33 ± 0.10	0.56	0.34	0.20 ± 0.01
$^{99}\mathrm{Y}_{60}$	1.48 ± 0.02	0.17	0.17	1.470 ± 0.007
$^{100g}\mathrm{Y}_{61}$	0.71 ± 0.03	0.35	0.18	0.735 ± 0.007
$^{101}\mathrm{Y}_{62}$	0.40 ± 0.02	0.14	0.13	0.448 ± 0.019
$^{102g}\mathrm{Y}_{63}$	0.29 ± 0.02	0.20	0.17	0.30 ± 0.01
$^{103}\mathrm{Y}_{64}$	0.23 ± 0.02	0.09	0.12	
$^{105}\mathrm{Zr}_{65}$	0.6 ± 0.1	0.10	0.09	$1.0^{+1.2}_{-0.4}$ [12]
$^{104g}\mathrm{Nb}_{63}$	5.0 ± 0.4	3.1	40.8	4.8 ± 0.4
$^{104m}\mathrm{Nb}_{63}$	1.0 ± 0.1			0.92 ± 0.04
$^{105}\mathrm{Nb}_{64}$	2.8 ± 0.1	4.2	3.92	2.95 ± 0.06
$^{106}\mathrm{Nb}_{65}$	0.90 ± 0.02	0.19	0.16	1.02 ± 0.05
$^{107}\mathrm{Nb}_{66}$	0.30 ± 0.03	0.78	0.68	0.33 ± 0.05 [12]
$^{108}\mathrm{Nb}_{67}$	0.19 ± 0.02	0.47	0.28	$0.20^{+0.03}_{0.02}$ [24]
$^{109}\mathrm{Nb}_{68}$	0.19 ± 0.03	0.46	0.18	
$^{110}\mathrm{Nb}_{69}$	0.17 ± 0.02	0.35	0.19	
$^{109}\mathrm{Tc}_{66}$	0.82 ± 0.10	0.36	0.38	0.86 ± 0.08
$^{110}\mathrm{Tc}_{67}$	0.78 ± 0.15	0.32	0.28	0.92 ± 0.03
$^{111}\mathrm{Tc}_{68}$	0.29 ± 0.02	0.19	0.18	0.30 ± 0.03
$^{112}\mathrm{Tc}_{69}$	0.23 ± 0.02	0.16	0.15	0.28 ± 0.03 [6]

TABLE II. List of P_n results. The QRPA predictions are calculated both with masses and deformations from the FRDM [4] and ETFSI [5] mass models. Experimental masses from [23] replaced the predicted ones whenever known. The literature values are taken from the most recent compilation of [17].

Isotope	P_n^{exp} (%)	P_n^{QRPA} FRDM (%)	P_n^{QRPS} ETFSI (%)	$P_n^{\mathrm{Lit.}}$ (%)
$^{99}\mathrm{Y}_{60}$	2.5 ± 0.5	0.2	0.3	1.9 ± 0.4
$^{100g}\mathrm{Y}_{61}$	1.8 ± 0.6	0.2	0.2	1.02 ± 0.07
$^{101}\mathrm{Y}_{62}$	1.5 ± 0.5	0.6	1.1	2.9 ± 0.7
$^{102g}\mathrm{Y}_{63}$	4.0 ± 1.5	1.6	2.5	6.0 ± 1.7
$^{103}\mathrm{Y}_{64}$	8.3 ± 3	4.2	8.0	
$^{104g}\mathrm{Nb}_{63}$	0.06 ± 0.03	0.0	0.2	
$^{104m}\mathrm{Nb}_{63}$	0.05 ± 0.03			
$^{105}\mathrm{Nb}_{64}$	1.7 ± 0.9	0.3	0.3	
$^{106}\mathrm{Nb}_{65}$	4.5 ± 0.3	0.3	0.8	
$^{107}\mathrm{Nb}_{66}$	6.0 ± 1.5	5.7	7.3	
$^{108}\mathrm{Nb}_{67}$	6.2 ± 0.5	15.6	5.6	
$^{109}\mathrm{Nb}_{68}$	31 ± 5	13.6	15.9	
$^{110}\mathrm{Nb}_{69}$	40 ± 8	19.0	92.0	
$^{109}\mathrm{Tc}_{66}$	0.08 ± 0.02	0.01	0.01	
$^{110}\mathrm{Tc}_{67}$	0.04 ± 0.02	0.22	0.09	
$^{111}\mathrm{Tc}_{68}$	0.85 ± 0.20	0.38	0.58	
$^{112}\mathrm{Tc}_{69}$	2.6 ± 0.5	0.90	1.11	

the ETFSI approach [5]. On the average, the predicted values follow the general trend of decreasing $T_{1/2}$ and increasing P_n values with increasing neutron number, but differ in the absolute values. The Y and Tc nuclei as well as ^{104}Nb and ^{106}Nb, but excluding ^{110}Tc, have longer $T_{1/2}$ and higher P_n values than predicted, whereas the heavy isotopes with $N \geq 66$, excluding ^{109}Nb, show the inverse behavior. The longer experimental $T_{1/2}$ together with the larger P_n value of $^{99}\mathrm{Y}_{60}$ are understood as being due to the coexistence of spherical and deformed shapes in the $N = 59$ β-decay daughter ^{99}Zr [19]. The treatment of shape coexistence is not foreseen in the standard QRPA. However, when simulating this effect by neglecting those calculated *deformed* GT transitions to low-lying states in ^{99}Zr which are experimentally known to be *spherical*, we obtain $T_{1/2}^{\mathrm{QRPA}} \simeq 2.2$ s and $P_n^{\mathrm{QRPA}} = (2\text{–}3)\%$. The calculated $T_{1/2}$ of $^{105}\mathrm{Zr}_{65}$ and $^{106}\mathrm{Nb}_{65}$ are too short by a factor of 5. This is observed for all $N = 65$ isotones with $Z \simeq 40$ and may be due to an incorrect placement of the $\nu s_{1/2}$ level in the folded Yukawa potential which becomes the valence orbital at $N = 65$, thus dominating the low-lying GT strength. However, as is indicated by the $I^{\pi} = 1/2^{+}$ ground states of the $N = 57$ isotones ^{95}Sr, ^{97}Zr, and ^{99}Mo [20], the $\nu s_{1/2}$ level lies below the $\nu g_{7/2}$ shell. In any case, a perfect agreement between the experiment and the above predictions [4,5] cannot be expected, since shape transitions in the $N \simeq 66$ midshell region are obviously not properly described in macroscopic-microscopic theories (see, e.g., discussion in the first part of [2]).

The systematically larger experimental P_n values (see Table II) seem to indicate a steeper decrease of the S_n values beyond $N \simeq 60$ than predicted. This trend is, however, requested from nuclear-structure arguments in the frame of the $N_p N_n$ systematics [21,22] as well as from astrophysical considerations [2]. The slightly better performance of the ETFSI model for the most neutron-rich isotopes investigated in this work is due to the prediction of somewhat higher Q_β and lower S_n values compared to the FRDM approach, thus leading to shorter $T_{1/2}$ and higher P_n's. The striking difference between the two theoretical P_n values for ^{110}Nb, for example, is due to the fact that the intense GT transitions (with $\log ft \simeq 4.3\text{–}4.8$) involving the $\pi g_{9/2}$ and the $\nu g_{7/2}$ partner orbitals are situated just below (FRDM) or just above (ETFSI) the predicted neutron separation energy (see Fig. 2). In general, the rather high P_n values observed indicate the increasing importance of fast β transitions to high-lying states of nuclei with large neutron excess.

The mass range covered in this work extended from $A = 99$ (Y) up to $A = 112$ (Tc). This allowed us to obtain the isotopic yield curves for fission products over this mass range. By unfolding the observed counting rates of the delayed neutron precursors for detection efficiency of the long-counter and P_n values determined in this work and

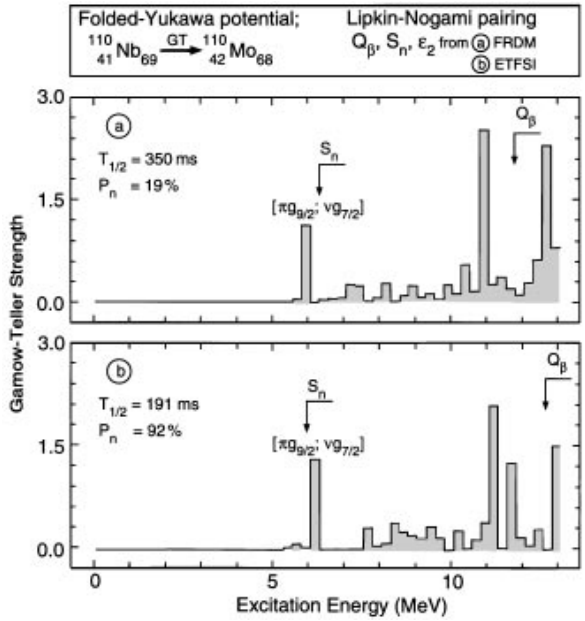

FIG. 2. Gamow-Teller (GT) strength functions for the decay of ^{110}Nb calculated with masses and deformations from the FRDM (upper part) and the ETFSI (lower part) mass models.

earlier, it was possible to extract the yield curves for Y, Nb, and Tc isotopes over a 3 orders of magnitude range. This provides for the first time high-quality data for testing the model calculations for the yields of very neutron-rich nuclei in fission and will make predictions even further out from the valley of stability more reliable [14]. Figure 3 shows the observed independent isotope yields for $^{99-103}$Y, $^{104-110}$Nb, and $^{109-112}$Tc isotopes, as well as the theoretical

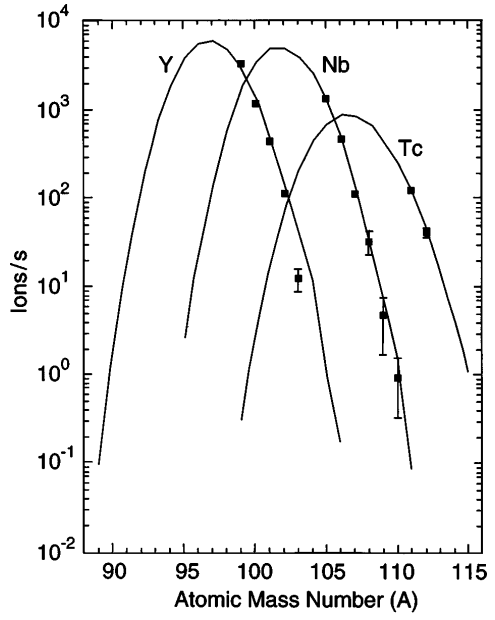

FIG. 3. Independent yields of Y, Nb, and Tc isotopes in fission induced by 25 MeV protons. The lines represent theoretical yields from the model of Rubchenya described in [14].

yields given by the model of Rubchenya described in [14]. The errors of the production rates of the most neutron-rich isotopes, especially ^{109}Nb and ^{110}Nb, are based on minimum-maximum yields deduced from the calibration of the detection efficiencies with the β-delayed neutron precursors ^{94}Rb and ^{95}Rb mentioned above. The production rate for ^{110}Nb of 1 ion/s represents at present the lowest limit of observation for neutron-rich nuclei at the new IGISOL facility.

The authors thank Dr. J. Persson for help during the measurements and the cyclotron staff. This work was supported by the Deutsche Akademische Austauschdienst and the Academy of Finland. One of us (P. D.) is grateful for the support by the Human Capital and Mobility program of the European Union.

*Electronic address: KLKRATZ@VKCMZD.CHEMIE.UNI-MAINZ.DE
†Electronic address: MMJH@JYFL.JYU.FI
‡Permanent address: St. Petersburg Nuclear Physics Institute, 188350, Gatchina, Russia.
§Permanent address: V. G. Khlopin Radium Institute, 194021, St. Petersburg, Russia.

[1] J. Dobaczewski *et al.*, Phys. Rev. Lett. **72**, 981 (1994); N. Fukunishi *et al.*, Phys. Lett. B **296**, 279 (1992).
[2] K.-L. Kratz *et al.*, Astrophys. J. **403**, 216 (1993); F.-K. Thielemann *et al.*, Nucl. Phys. **A570**, 329c (1994); K.-L. Kratz, in *Nuclei in the Cosmos III*, AIP Conf. Proc. No. 327 (AIP, New York, 1995), p. 113.
[3] B. Chen *et al.*, Phys. Lett. B **355**, 37 (1995).
[4] P. Möller *et al.*, At. Data Nucl. Data Tables **59**, 185 (1995).
[5] Y. Abousir *et al.*, At. Data Nucl. Data Tables **61**, 127 (1995).
[6] J. Äystö *et al.*, Nucl. Phys. **A515**, 365 (1990).
[7] J. A. Shannon *et al.*, Phys. Lett. B **336**, 136 (1994).
[8] S. Schoedder *et al.*, Z. Phys. A **352**, 237 (1995).
[9] W. B. Walters, in *Procedings of the International Symposium on Nuclear Physics of Our Times* (World Scientific, Singapore, 1993), p. 457, ISBN 981-02-1358-1.
[10] K.-L. Kratz *et al.*, Nucl. Phys. **A417**, 447 (1984).
[11] P. Möller and J. Randrup, Nucl. Phys. **A514**, 1 (1990).
[12] J. Äystö *et al.*, Phys. Rev. Lett. **69**, 1167 (1992).
[13] M. Bernas *et al.*, Phys. Lett. B **331**, 19 (1994).
[14] P. P. Jauho *et al.*, Phys. Rev. C **49**, 2036 (1994).
[15] P. Taskinen *et al.*, Nucl. Instrum. Methods Phys. Res., Sect. A **281**, 539 (1989).
[16] P. L. Reeder *et al.*, in *Proceedings of the Specialists' Meeting on Delayed Neutron Properties, 1986* (Univ. of Birmingham, Birmingham, England, 1986), p. 37, ISBN 07044 0926 7.
[17] G. Rudstam *et al.*, At. Data Nucl. Data Tables **53**, 1 (1993).
[18] B. Pfeiffer *et al.*, in Ref. [16], p. 75.
[19] G. Lhersonneau *et al.*, Phys. Rev. C **49**, 1379 (1994).
[20] K.-L. Kratz *et al.*, Z. Phys. A **312**, 43 (1983).
[21] R. F. Casten, Phys. Rev. Lett. **54**, 1991 (1985).
[22] P. E. Haustein *et al.*, Phys. Rev. C **38**, 467 (1988).
[23] G. Audi and A. H. Wapstra, Nucl. Phys. **A565**, 1 (1993).
[24] H. Penttilä *et al.* (to be published).